Heat coupled Gaussian continuous-wave double-pass type-II second harmonic generation: inclusion of thermally induced phase mismatching and thermal lensing

Mohammad Sabaeian,[*] **Fatemeh Sedaghat Jalil-Abadi, Mostafa Mohammad Rezaee, and Alireza Motazedian**

Department of Physics, Faculty of Science, Shahid Chamran University of Ahvaz, Ahvaz, Iran
[*]*sabaeian@scu.ac.ir*

Abstract: A model describing the thermal effects in type II second harmonic generation (SHG) of Gaussian continuous-wave (CW) in a double-pass cavity is presented. The thermally induced phase mismatching (TIPM) along with thermal lensing was included in the classical SHG formalism through the interposing the heat and TIPM equations. To this end, eight equations were coupled together and solved simultaneously to reveal how the SHG is affected in time when heat is generated in the crystal. The model showed an excellent agreement with experimental data [Opt. Laser Tech. **34**, 333–336 (2002)]. Furthermore, a numerical procedure, which was developed in this work, is introduced for simultaneously solving the SHG, heat, and TIPM equations with home-used computing machines.

OCIS codes: (190.0190) Nonlinear optics; (140.6810) Thermal effects.

References and links

1. J. Golden, "Green lasers score good marks in semiconductor material processing," Laser Focus World **28**, 75 (1992).
2. R. J. Rockwell, Jr., "Designs and functions of laser systems for biomedical applications," Ann. N. Y. Acad. Sci. **168**(3), 459–471 (1969).
3. I. C. Frennesson and S. E. Nilsson, "Effects of argon (green) laser treatment of soft drusen in early age-related maculopathy: a 6 month prospective study," Br. J. Ophthalmol. **79**(10), 905–909 (1995).
4. J. D. Bierlein and H. Vanherzeele, "Potassium titanyl phosphate: properties and new applications," J. Opt. Soc. Am. B **6**(4), 622–633 (1989).
5. Y. F. Lu, S. M. Huang, and Z. Sun, "Raman spectroscopy of phenylcarbyne polymer films under pulsed green laser irradiation," J. Appl. Phys. **87**(2), 945–951 (2000).
6. T. Wiener and S. Karp, "The role of blue/green laser systems in strategic submarine communications," IEEE Trans. Commun. **28**(9), 1602–1607 (1980).
7. B. Hitz, "Green lasers gear up for display markets," Opt. Laser Eur. **173**, 21–26 (2009).
8. P. E. Möbert, E. Heumann, G. Huber, and B. H. T. Chai, "Green Er^{3+}:$YLiF_4$ upconversion laser at 551nm with Yb^{3+} codoping: a novel pumping scheme," Opt. Lett. **22**(18), 1412–1414 (1997).
9. J. Zheng, S. Zhao, Q. Wang, X. Zhang, and L. Chen, "Influence of thermal effect on KTP type-II phase-matching second-harmonic generation," Opt. Commun. **199**(1–4), 207–214 (2001).
10. D.-G. Xu, J.-Q. Yao, B.-G. Zhang, R. Zhou, E. Li, S.-Y. Zhao, X. Ding, W.-Q. Wen, Y.-X. Niu, J. Hu, and P. Wang, "110 W high stability green laser using type II phase matching KTiOPO4 (KTP) crystal with boundary temperature control," Opt. Commun. **245**(1–6), 341–347 (2005).
11. D. Zhang, J. Lu, B. Feng, and J. Zhang, "Increased temperature bandwidth of second harmonic generator using two KTiOPO4 crystals cut at different angles," Opt. Commun. **281**(10), 2918–2922 (2008).
12. D. W. Feng, Y. Feng, and G. W. Zhang, "Efficient $Nd:Y_{0.5}Gd_{0.5}VO_4$-$KTiOPO_4$ green laser under diode pumping into the emitting level $^4F_{3/2}^1$," Laser Phys. **22**(5), 888–891 (2012).
13. T. Harimoto, B. Yo, and K. Uchida, "Compensation for the thermal effect in the second-harmonic generation of a Q-switched nanosecond-kilohertz Nd:YVO4 lasers," Opt. Rev. **19**(5), 341–344 (2012).

14. K. Regelskis, J. Želudevičius, N. Gavrilin, and G. Račiukaitis, "Efficient second-harmonic generation of a broadband radiation by control of the temperature distribution along a nonlinear crystal," Opt. Express **20**(27), 28544–28556 (2012).
15. J. Bai and G. Chen, "Continuous-wave diode-laser end-pumped Nd:YVO$_4$/KTP high-power solid-state green laser," Opt. Laser Technol. **34**(4), 333–336 (2002).
16. S. C. Kumar, G. K. Samanta, K. Devi, and M. Ebrahim-Zadeh, "High-efficiency, multicrystal, single-pass, continuous-wave second harmonic generation," Opt. Express **19**(12), 11152–11169 (2011).
17. T. Sekine, H. Sakai, Y. Takeuchi, Y. Hatano, T. Kawashima, H. Kan, J. Kawanaka, N. Miyanaga, and T. Norimatsu, "High efficiency 12.5 J second-harmonic generation from CsLiB6O$_{10}$ nonlinear crystal by diode-pumped Nd:glass laser," Opt. Express **21**(7), 8393–8400 (2013).
18. H. Kiriyama, N. Inoue, and K. Yamakawa, "High energy second-harmonic generation of Nd:glass laser radiation with large aperture CsLiB6O$_{10}$ crystals," Opt. Express **10**(19), 1028–1032 (2002).
19. M. Aoyama, T. Harimoto, J. Ma, Y. Akahane, and K. Yamakawa, "Second - harmonic generation of ultra-high intensity femtosecond pulses with a KDP crystal," Opt. Express **9**(11), 579–585 (2001).
20. A. Singh, P. K. Mukhopadhyay, S. K. Sharma, K. Ranganathan, and S. M. Oak, "82 W continuous-wave green beam generation by intracavity frequency doubling of diode-side-pumped Nd: YAG Laser," IEEE Quantum Electron. **47**(3), 398–405 (2011).
21. P. F. Zhu, B. Li, W. Q. Liu, T. H. Liu, C. X. Fang, Y. Zhao, and Q. Zheng, "All solid state continuous wave frequency doubling Nd:YAG/LBO laser with 8.2 W output power at 660 nm," Opt. Spectrosc. **113**(5), 560–564 (2012).
22. X. Yang, L. Song, and L. X. Zhang, "All solid state continuous wave frequency doubling Nd:LuVO4/GBCOB laser at 533 nm," Laser Phys. **22**(5), 836–838 (2012).
23. M. Sabaeian, L. Mousave, and H. Nadgaran, "Investigation of thermally-induced phase mismatching in continuous-wave second harmonic generation: A theoretical model," Opt. Express **18**(18), 18732–18743 (2010).
24. A. G. Getman, S. V. Popov, and J. R. Taylor, "7 W average power, high-beam-quality green generation in MgO-doped stoichiometric periodically poled lithium tantalite," Appl. Phys. Lett. **85**(15), 3026–3028 (2004).
25. T. Mizushima, H. Furuya, S. Shikii, K. Kusukame, K. Mizuuchi, and K. Yamamoto, "Second harmonic generation with high conversion efficiency and wide temperature tolerance by multi-pass scheme," Appl. Phys. Express **1**, 032003 (2008).
26. Zh. W. Chao, Y. H. An, Y. M. Andreev, S. G. Grechin, and G. V. Lanskii, "Simulation of thermo-optic coupling in the thermally anisotropic gallium selenide crystal for second harmonic generation," Laser Phys. Lett. **11**(7), 075402 (2014).
27. Y. Liang, R. Su, L. Lu, and H. Liu, "Temperature non-uniformity occurring during the cooling process of a KDP crystal and its effects on second harmonic generation," Appl. Opt. (Accepted to be published, 2014).
28. S. G. Sabouri, S. C. Kumar, A. Khorsandi, and M. Ebrahim-Zadeh, "Thermal effects in high-power continuous-wave single-pass second harmonic generation," IEEE J. Sel. Top. Quantum Electron. **20**(5), 7500210 (2014).
29. M. Sabaeian, "Analytical solutions for anisotropic time-dependent heat equations with Robin boundary condition for cubic-shaped solid-state laser crystals," Appl. Opt. **51**(30), 7150–7159 (2012).
30. C. A. Klein, "Optical distortion coefficients of high-power laser windows," Opt. Eng. **29**(4), 343–350 (1990).
31. C. A. Klein, "Oxyfluoride glass for high-energy laser windows: Thermal lensing issue," Appl. Phys. Lett. **87**(23), 231117 (2005).
32. C. Pfistner, R. Weber, H. Weber, S. Merazzi, and R. Gruber, "Thermal beam distortions in end-pumped Nd: YAG, Nd: GSGG, and Nd: YLF rods," IEEE J. Quantum Electron. **30**(7), 1605–1615 (1994).
33. L. Mousavi, M. Sabaeian, and H. Nadgaran, "Thermally-induced birefringence in solid-core photonic crystal fiber lasers," Opt. Commun. **300**, 69–76 (2013).
34. W. Xie, S.-C. Tam, Y.-L. Lam, J. Liu, H. Yang, J. Gu, and W. Tan, "Influence of the thermal effect on the TEM$_{00}$ mode output power of a laser-diode side-pumped solid-state laser," Appl. Opt. **39**(30), 5482–5487 (2000).
35. R. Lausten and P. Balling, "Thermal lensing in pulsed laser amplifiers: an analytical model," J. Opt. Soc. Am. B **20**(7), 1479–1485 (2003).
36. A. K. Cousins, "Temperature and thermal stress scaling in finite-length end-pumped laser rods," IEEE J. Quantum Electron. **28**(4), 1057–1069 (1992).
37. L. C. Malacarne, N. G. C. Astrath, and L. S. Herculano, "Laser-induced wavefront distortion in optical materials: a general model," J. Opt. Soc. Am. B **29**(12), 3355–3359 (2012).
38. M. Sabaeian and H. Nadgaran, "Bessel-Gauss beams: Investigation of thermal effects on their generation," Opt. Commun. **281**(4), 672–678 (2008).
39. H. Nadgaran, M. Servatkhah, and M. Sabaeian, "Mathieu-Gauss beams: A thermal consideration," Opt. Commun. **283**(3), 417–426 (2009).
40. L. Mousavi, M. Sabaeian, and H. Nadgaran, "Numerical modeling of self-heating effects on guiding modes of high-power photonic crystal fiber lasers," Lithuanian J. Phys. **53**(2), 104–111 (2013).
41. M. Sabaeian, H. Nadgaran, M. De Sario, F. Prudenzano, and L. Mecia, "Thermal effects on octagonal double clad Yb:glass fiber laser," Opt. Mater. **29**, 5336 (2008).
42. M. Sabaeian and H. Nadgaran, "Investigation of thermal dispersion and thermally-induced birefringence on high-power double clad Yb:glass fiber laser," IJOP **2**, 25–31 (2008).

43. M. Liao, S. A. Payne, J. Dawson, A. Drobshoff, C. Ebbers, D. Pennington, and L. Taylor, "Thermally induced dephasing in periodically poled KTP frequency-doubling crystals," J. Opt. Soc. Am. B **21**(12), 2191–2196 (2004).
44. G. Mann, S. Seidel, and H. Weber, "Influence of mechanical stress on the conversion efficiency of KTP and LBO," in *Industrial Lasers and Inspection (EUROPTO Series)* (1999), pp. 289–297.
45. R. W. Boyd, *Nonlinear Optics*, 3rd ed. (Academic, 2008), Chap. 2.

1. Introduction

Green light lasers have found potential applications in material processing [1], biomedicine [2], ophthalmology [3], printing [4], spectroscopy [5], underwater communications [6], display technology [7], and pumping sources for solid-state lasers [8]. One of the favorable and efficient ways to generate green light is nonlinear processes through the second harmonic generation (SHG) of fundamental wave of 1064 nm. In this regard, high efficient outputs with good beam quality are of great importance. One of the famous and useful nonlinear crystals capable of converting 1064 nm beams into 532 nm is $KTiOPO_4$ (KTP) crystal, possessing high nonlinear convection coefficient (d_{eff} = 7.3 pm/V), high acceptance angles, high threshold damage, high thermal conductivity [9], and small walking-off angle [10]. The transmission band of KTP ranges from 350 to 4400 nm, covering ultraviolet to infrared range of the spectrum [4]. The matching range of KTP crystal ranges from 990 to 3300 nm [4]. With respect to these remarkable properties, KTP is an excellent choice to be used as a green light source pumped with outputs of solid-state lasers such as Nd:YAG and Nd:YVO$_4$ [11].

Over the years, various theoretical and experimental efforts have been made to increase the SHG efficiency [12-16]. In extracavity configuration in which the fundamental wave generator is external to the nonlinear cavity, pulsed SHG efficiencies as high as 70% [13], 71.5% [17], 74% [18] and 80% [19] have been reported. In CW operation, however, considerably lower efficiencies such as 11% [20], 21.5% [21], 23.6% [12], 25.5% [15], and 28.5% [22] for conventional and single crystal cavity have been reported. In CW SHG, we encounter longer interaction lengths compared to pulsed regime, that is, the energy exchange between the fundamental and second harmonic waves get complete in longer lengths. Therefore, reaching to higher second harmonic efficiency is a harder task. Interaction length which is defined as $l = \sqrt{\varepsilon_0 c^3 (n^{\omega_1})^2 n^{\omega_2} / 4\omega_1^2 d_{eff}^2 I}$ [23] with ε_0, c, n^{ω_1}, n^{ω_2}, ω_1, d_{eff}, and I as the vacuum permittivity, speed of light, refractive index of fundamental wave, refractive index of second harmonic wave, fundamental wave frequency, effective nonlinear coefficient, and fundamental beam intensity, respectively, reveals that in CW regime, in order to enhance the SHG efficiency, the fundamental beam intensity should be rather increased. However, the thermal effects accompanying with escalation of pump intensity prevent further enhancement of SHG efficiency through thermally induced phase mismatching (TIPM) and thermal lensing. The former perturbs the phase matching and the latter reduces the beam quality and may make the resonator unstable, if high powers are used. In fact, as we will see later, a competition between TIPM and interaction length, former towards reduction and the latter towards increase in SGH efficiency, occurs. In order to obtain the highest possible SHG efficiency, an optimization between the fundamental beam power and beam spot size should be done in each crystal length.

At first glance it seems that by enlarging the crystal length, one can provide the distance long enough to complete the nonlinear interaction and reducing the temperature, providing the condition of increase in nonlinear conversion efficiency. But, this way may propose unrealistic crystal length. Furthermore, long crystals absorb more fundamental and second harmonic energy.

Apart from periodically poled crystals developed recently in which quasi-phase phase matching technique is employed [24], for conventional crystals, two effective schemes have been proposed earlier to allow the nonlinear interaction to be completed: the use of double-pass cavity that doubles the effective crystal length and successive single-pass cavities [16,

25]. Kumar *et al.* obtained >55% conversion efficiency for CW single-pass multicrystal SHG using MgO:sPPLT [16]. The use of double-pass cavity provides a cheap and simpler scheme for achieving higher SHG efficiency. This can be done by placing a high reflective (HR) mirror at one end of the cavity to return back the residual fundamental wave to complete its interaction with second harmonic wave [12,15]. Nevertheless, the loss of phase matching in systems which is heated has been introduced as the most limiting factor to get higher efficiencies, those predicted by theoretical models [13,23,26,27]. For a crystal which is phase matched at a specific temperature, for example at 298 K, depending on the pump power used, a non-uniform temperature distribution is established throughout the crystal which is responsible for phase mismatching [27]. Zhang Wen Chao *et al.* [26] concluded in their modeling, which is performed for a gallium Selenide crystal pumped with pulsed CO_2, that the controlling TIPM is an effective contrivance to prevent reduction in SHG efficiency due to thermal effects. Several approaches have been proposed to suppress the thermal effects. Placing the crystal in an oven and keeping it in an optimized temperature has been reported by Singh *et al.* [20], Sabouri *et al.* [28], and Harimoto *et al.* [13].

A perfect cooling system [29] which is thought to be capable to solve the heat problem cannot be completely happen because of finite relaxation time of heat dissipation in the crystal. This idea can partially reduce the detrimental thermal effects. Other effects which are induced by heat are thermally induced bulging and stress leading to other contributions in thermal lensing [30,31]. Klein [31] reported that these two terms can be important for oxylfuride glass. However, for KTP crystal, due to the smallness of Young's modulus and thermal expansion coefficient by two and one order of magnitude, respectively, than those of oxyfluride, our calculations show that the dn/dT effects are greater than the bulging and stress significantly. Stress can introduce birefringence in long-length fibers [32,33], that is, a new component orthogonal to initially polarized electric field component is produced [36]. However, for crystals it has been shown that the stress induced changes in refractive indices are sufficiently lower than that of dn/dT [32-36]. Thermal stresses can be important in material of thickness within the long-rod or thin-disk approximations [37]. Thermal lensing which is usually investigated by ABCD matrix method [38,39] when perfect lens is assumed, has shown to be another detrimental thermal effect leading to degradation in beam quality. As calculations indicated, when a Gaussian pump is applied, the aberrations in thermal lens do not allow using ABCD method. Therefore, the inclusion of thermal lensing with its aberrations requires that Maxwell's wave equations with considering temperature dependence of refractive index should be solved [40-42].

We, in our previous work [23], have made a model to include the thermal effects in CW single-pass type II SHG. As for describing ideal single-pass type II SHG, three coupled equations are required, to include the thermal effects two more equations of heat and TIPM have been added to get a set of five coupled equations. Our model was adopted successfully to a type I quasi-phase matched crystal by Sabouri *et al.* [28]. A short pulsed version of our work [23] has been used by Regelskis *et al.* to enhance the SHG efficiency [14]. Liao *et al.* developed a thermal model for PPKTP in a single-pass configuration and confirmed it with experimental data [43]. They observed a reduction in conversion efficiency with elapsing time.

In this work, we develop a model to show how the CW double-pass SHG process is affected by generating the heat within the nonlinear crystal. The maximum efficiency versus the pump power and beam spot size is calculated for a KTP crystal. We will discuss the effect of crystal length in the problem. As shown by Mann *et al.* [44], the thermal stresses are negligible for KTP, so that we neglected them in our model. Unlike our previous model which was performed for a steady-state regime, the present work considers the time evolution of SHG when the crystal is gradually warmed up. The results will be compared with experimental results reported by Bai *et al.* for a double-pass configuration [15]. The model has been established on eight coupled equations required to be solved simultaneously to

investigate the mutual effects of heat and SHG in type II double-pass configuration. Furthermore, we present a numerical procedure to solve these eight coupled equations with home-used computing machines.

Our eight coupled equations model adopted to describe CW double-pass type II systems has been arranged as follows: two forward and backward fundamental wave equations with ordinary polarization, two forward and backward fundamental waves with extraordinary polarization, two forward and backward second harmonic wave equations with extraordinary polarization, one heat equation, and one thermally induced phase mismatching equation. Thermal lensing through inclusion of temperature-dependent refractive index in the wave equations will be considered automatically. As the simultaneous solving of these equations, which are inherently different in type, is a time- and RAM- consuming process, a numerical procedure was developed and will be introduced allowing the program to be solved with home-used computational machines.

2. The theory of heat coupled CW double-pass type II SHG

2.1 Double-pass type II SHG equations without heat effect

In type II SHG, the two orthogonal fundamental electric filed vectors coincide with ordinary and extraordinary direction of refractive indices. The phase matching condition is satisfied for second harmonic electric field vector laying on the extraordinary direction such that the condition of $n^o \omega_1 + n^e \omega_1 = n^e \omega_2$ is fulfilled [23]. This is equivalent to $\Delta k = 0$. Therefore, in type II configuration, we encounter with three waves travelling and interacting together along the crystal length. The sum frequency generation formalism can be well adopted to describe this phenomenon with equal fundamental wave's frequencies [23].

If the propagating waves are assumed to be $\tilde{\mathbf{E}}_i(r,z,t) = E_i(r,z)e^{i(k_i z - \omega_i t)} + C.C$ where C.C. is the complex conjugate [45] with $i = 1,2$ referring to fundamental waves and $i = 3$ to second harmonic wave, then, the type II SHG for a single-pass cavity is described through the set of following equations [23]:

$$\frac{dE^{o,\omega}}{dz} - \frac{ic}{2n^{o,\omega}\omega}\nabla_T^2 E^{o,\omega} + \frac{\gamma_1}{2}E^{o,\omega} = \frac{2i\omega d}{n^{o,\omega}c}E^{e,2\omega}E^{*e,\omega}e^{-i\Delta k z} \tag{1}$$

$$\frac{dE^{e,\omega}}{dz} - \frac{ic}{2n^{e,\omega}\omega}\nabla_T^2 E^{e,\omega} + \frac{\gamma_2}{2}E^{e,\omega} = \frac{2i\omega d}{n^{e,\omega}c}E^{e,2\omega}E^{*o,\omega}e^{-i\Delta k z} \tag{2}$$

$$\frac{dE^{e,2\omega}}{dz} - \frac{ic}{4n^{e,2\omega}\omega}\nabla_T^2 E^{e,2\omega} + \frac{\gamma_3}{2}E^{e,2\omega} = \frac{4id\omega}{n^{e,2\omega}c}E^{o,\omega}E^{e,\omega}e^{+i\Delta k z} \tag{3}$$

In the equations above, ∇_T^2 is the transverse Laplacian, γ_1 and γ_2 are the absorption coefficients of fundamental waves and γ_3 is of second harmonic wave, d_{eff} is the effective nonlinear coefficient, and ω is the angular frequency of fundamental waves.

If the backward fundamental waves are also considered which are caused by reflecting the residual fundamental waves and generated second harmonic wave by a high reflecting mirror, the set of equations above doubles. For the future numerical considerations, we use the change of variable given as follow:

$$E_{\pm}^{o,\omega}(r,z) = \sqrt{\frac{P_F}{2n^{o,\omega}c\varepsilon_0\pi\omega_f^2}}\psi_{1\pm}(r,z) \tag{4}$$

$$E_\pm^{e,\omega}(r,z) = \sqrt{\frac{P_F}{2n^{e,\omega}c\varepsilon_0\pi\omega_f^2}}\psi_{2\pm}(r,z) \tag{5}$$

$$E_\pm^{e,2\omega}(r,z) = \sqrt{\frac{P_F}{n^{e,2\omega}c\varepsilon_0\pi\omega_s^2}}\psi_{3\pm}(r,z) \tag{6}$$

where 1, 2, and 3 refer to ordinary fundamental wave, extraordinary fundamental wave, and extraordinary second harmonic wave, respectively. P_F is the power of each fundamental wave component at the entrance face, $z = 0$, and ω_f and ω_s are the fundamental and second harmonic wave beam spot sizes, respectively, which are assumed to be equal and constant over the nonlinear crystal, since the crystal length is several times greater than Reighley range. With above definitions, ψ's become dimensionless quantities and $|\psi_i|^2$'s denote the efficiencies, i.e. $|\psi_{1,2\pm}|^2 = I_{1,2\pm}/I_F(z=0)$ for fundamental waves and $|\psi_{3\pm}|^2 = I_{3\pm}/2I_F(z=0)$ for second harmonic waves. The value of 2 at the denominator insures us that the "total" fundamental intensity is considered. With assumptions above, the coupled wave equations for describing double-pass type II SHG become:

$$\pm\frac{d\psi_{1\pm}(r,z)}{dz} - \frac{ic}{2n^{o,\omega}\omega}\nabla_T^2\psi_{1\pm}(r,z) + \frac{\gamma_1}{2}\psi_{1\pm}(r,z) = \frac{i}{l}\psi_{3\pm}(r,z)\psi_{2\pm}^*(r,z)e^{\mp i\Delta kz} \tag{7}$$

$$\pm\frac{d\psi_{2\pm}(r,z)}{dz} - \frac{ic}{2n^{e,\omega}\omega}\nabla_T^2\psi_{2\pm}(r,z) + \frac{\gamma_2}{2}\psi_{2\pm}(r,z) = \frac{i}{l}\psi_{3\pm}(r,z)\psi_{1\pm}^*(r,z)e^{\mp i\Delta kz} \tag{8}$$

$$\pm\frac{d\psi_{3\pm}(r,z)}{dz} - \frac{ic}{4n^{e,2\omega}\omega}\nabla_T^2\psi_{3\pm}(r,z) + \frac{\gamma_3}{2}\psi_{3\pm}(r,z) = \frac{i}{l}\psi_{1\pm}(r,z)\psi_{2\pm}(r,z)\,e^{\pm i\Delta kz} \tag{9}$$

For the fundamental and second harmonic waves, the Gaussian waves at the plane of $z = 0$ are considered to be $\psi_{1,2+}(z=0) = \exp\left(-r^2/\omega_f^2\right)$ and $\psi_{3+}(z=0) = 0$, respectively. At the end of the cavity ($z = l$), the conditions of $\psi_{1,2-}(z=l) = \sqrt{R_{f,FW}}\psi_{1,2+}(z=l)$, and $\psi_3(z=l) = \sqrt{R_{f,SHW}}\psi_{3+}(z=l)$ are used where $R_{f,FW}$ and $R_{f,SHW}$ are the reflective powers of forward mirrors at fundamental and second harmonic wavelengths, respectively. In Eqs. (7)–(9), the term $\Delta k = k_1 + k_2 - k_3$ is the wave vector mismatching. We assume that in a specific temperature, T_0, the crystal is phase matched. However, when the crystal refractive indices are changed due to the temperature increase, we used $\Delta\varphi = \int_0^z \Delta k(T)\,dz'$ as the thermally induced phase mismatching (TIPM). For type II SHG, $l = \sqrt{\varepsilon_0 c^3\, n^{e,\omega}\, n^{o,\omega}\, n^{e,2\omega}\, \pi\,\omega_f^2/4\omega^2 d_{eff}^2 P_F}$ is interoperated as interaction length, that is, a length scale determining the amount of energy exchange between the fundamental and second harmonic waves. According to this parameter, apart from inherent role of effective nonlinear coefficient, the beam spot size, ω_f, and the initial fundamental power, P_F, play the most important role in determining the SHG efficiency.

2.2 Heat and thermally induced phase mismatching equations

Optical absorption of fundamental and second harmonic waves when passing through the nonlinear crystal leads to heating. Hence, the forward and backward fundamental and second

harmonic waves can establish the heat source. In order to investigate the effects of heat on second harmonic profile and efficiency, the temperature distribution within the crystal must be known. This is necessary to calculate the TIPM and thermal lensing. Conduction heat equation allows this calculation which is given by [16]:

$$\rho C \frac{\partial T}{\partial t} - \vec{\nabla}.[K(T)\vec{\nabla}T] = S \qquad (10)$$

where ρ is the crystal mass density, C is the specific heat, $K(T) = K_0 / (T_0 + \Delta T)$ is the temperature-dependent thermal conductivity, and S is the heat source (density). Heat source term interconnects the wave equations, Eqs. (7)–(9), with heat equation, Eq. (10). Since all travelling waves contribute in the heat generation, the source term can be written as:

$$S = \gamma_1(I_+^{o,\omega} + I_-^{o,\omega}) + \gamma_2(I_+^{e,\omega} + I_-^{e,\omega}) + \gamma_3(I_+^{e,2\omega} + I_-^{e,2\omega}) \qquad (11)$$

As the wave intensity is given by $I = 2nc\varepsilon_0 \, |E|^2$, according to Boyd's notation, the heat equation takes the following form:

$$\rho c \frac{\partial T}{\partial t} - \vec{\nabla}.[K(T)\vec{\nabla}T] = \frac{P_F}{\pi \omega_F^2}\Big[\gamma_1(|\psi_{1+}|^2 + |\psi_{1-}|^2)$$
$$+ \gamma_2(|\psi_{2+}|^2 + |\psi_{2-}|^2) + 2\gamma_3(|\psi_{3+}|^2 + |\psi_{3-}|^2) \Big] \qquad (12)$$

The temperature boundary conditions for end faces and lateral surface have been taken from the following equation [29]:

$$-K(T)\hat{\mathbf{n}}. \nabla T\big|_{boundray} = h(T - T_\infty)_{boundray} + \sigma\varepsilon(T^4 - T_s^4)_{boundray} \qquad (13)$$

where $\hat{\mathbf{n}}$ is the outward vector perpendicular to the surface, h is the heat convection constant ($h = 10 W / m^2 / K$) [29], ε is surface emissivity ($\varepsilon = 0.9$), $\sigma = 5.669 \times 10^{-8} W / m^2 / K^4$ is the Stefan-Boltzmann constant, and T_∞ and T_S are the temperature of cooling fluid and ambient, respectively. For end faces the radiation has been taken into account, but for lateral surface the constant boundary condition ($T(t, r = a) = T_0$) is used.

Therefore, as above equation shows, heat is coupled to the wave equations through ψ_i's. But how does the heat equation affect the second harmonic generation? This question can be answered through the effects of heat on the refractive indices. This can be expressed by Taylor expansion of refractive index around the phase matching temperature, T_0, as $n_i(\lambda,T) = n_i(\lambda,T_0) + (dn_i / dT)(T - T_0)$ where i refers to principal coordinates, X, Y, and Z, of refractive index. For KTP crystal, the dn_i / dT coefficients are given by [23]:

$$\frac{dn_X}{dT} = (0.1323\lambda^{-3} - 0.4385\lambda^{-2} + 1.2307\lambda^{-1} + 0.7709) \times 10^{-5} (^\circ C^{-1}) \qquad (14)$$

$$\frac{dn_Y}{dT} = (0.5014\lambda^{-3} - 2.0030\lambda^{-2} + 3.3016\lambda^{-1} + 0.7498) \times 10^{-5} (^\circ C^{-1}) \qquad (15)$$

$$\frac{dn_Z}{dT} = (0.3896\lambda^{-3} - 1.3332\lambda^{-2} + 2.2762\lambda^{-1} + 2.1151) \times 10^{-5} (^\circ C^{-1}) \qquad (16)$$

The dn / dT coefficient can be simply calculated for every wavelength. However, the relations above are not applicable directly, because they are given in principal coordinates

while crystal is cut in specific angles of θ and ϕ and the waves are coincided on the ordinary and extraordinary directions. Ordinary and extraordinary refractive indices can be calculated via the following relation:

$$n = \frac{\sqrt{2}}{\sqrt{-B \pm \sqrt{B^2 - 4C}}} \tag{17}$$

where "$+$" and "$-$" signs refer to ordinary and extraordinary refractive indices, respectively. B and C are given by:

$$B = -\sin^2\theta\cos^2\phi(b+c) - \sin^2\theta\sin^2\phi(a+c) - \cos^2\theta(a+b) \tag{18}$$

and

$$C = \sin^2\theta\cos^2\phi\,bc + \sin^2\theta\sin^2\phi\,ac + \cos^2\theta\,ab \tag{19}$$

with $a = n_X^{-2}$, $b = n_Y^{-2}$, and $c = n_Z^{-2}$.

At any temperature rather than phase matching temperature, T_0, the relation of $\Delta k(T) = k_1(T) + k_2(T) - k_3(T) = 0$ cannot be longer satisfied. With the help of $k_i = 2\pi n_i / \lambda_i$, the phase mismatching due to temperature increase can be written as

$$\Delta k(T) = \frac{2\pi}{\lambda_1} n_1(T) + \frac{2\pi}{\lambda_2} n_2(T) - \frac{2\pi}{\lambda_3} n_3(T) \tag{20}$$

where we have used $n_1 = n^{o,\omega}$, $n_2 = n^{e,\omega}$, and $n_3 = n^{e,2\omega}$. Therefore, the TIPM can be written as:

$$\Delta\varphi = \int_0^z \left[\frac{2\pi}{\lambda_1} n^{o,\omega}(T) + \frac{2\pi}{\lambda_2} n^{e,\omega}(T) - \frac{2\pi}{\lambda_3} n^{e,2\omega}(T) \right] dz \tag{21}$$

Or in the differential form as

$$\frac{\Delta\varphi}{dz} = \frac{2\pi}{\lambda_1} n^{o,\omega}(T) + \frac{2\pi}{\lambda_2} n^{e,\omega}(T) - \frac{2\pi}{\lambda_3} n^{e,2\omega}(T) \tag{22}$$

Therefore the heat interposes the wave equations through the TIPM.

We summarize the treatment accomplished so far: In one hand, Eq. (22), i.e. TIPM equation, perturbs the SHG process through a mismatched phase apparent in the exponential. On the other hand, the fundamental as well as the second harmonic wave determine the heat source. Therefore, simultaneous solving of SHG, heat, and TIPM equations would give us a realistic answer.

4. Results

4.1 Experimental specifications

In order to realize our model and confirm it with experimental results, the specifications of Bai and Chen experiment were used [15]. A typical scheme is illustrated in Fig. 1. A double-pass cavity scheme is provided with a convex lens (M$_3$) with inner radius of curvature of 100 mm and a concave mirror (M$_4$) with a radius of curvature of 50 mm. This configuration for frequency-doubling crystal provides a minimum spot size inside and not at the end of the cavity. The crystal is placed at the waist position between the lens and mirror. We will see that in theory, how much is important of beam spot size in obtaining as high as possible green

power. The 1064 nm fundamental beam comes out from a two-end pumped Nd:YVO$_4$ crystal with a TEM$_{0,0}$ mode in a very wide pumping power range (that is not shown in Fig. 1). A KTP crystal with phase matching angles of $\theta = 90°$ and $\phi = 23.4°$ and a length of $l = 9mm$ was placed in the double-pass cavity. M$_3$ as the output coupler, is HR-coated at 1064 nm and HT-coated at 532 nm on the curved face. M$_4$ is coated as highly reflected at both 1064 and 532 nm. The KTP crystal is wrapped with an indium foil and inlaid in a water-cooled copper block ensuring sufficient cooling. In our modeling with accordance to the experiment, we took the crystal surface temperature to be constant at 298 K. In practice, to get a higher SHG efficiency, small spot sizes of the order of 30 to $50 \mu m$ are used [16] to reduce the interaction length.
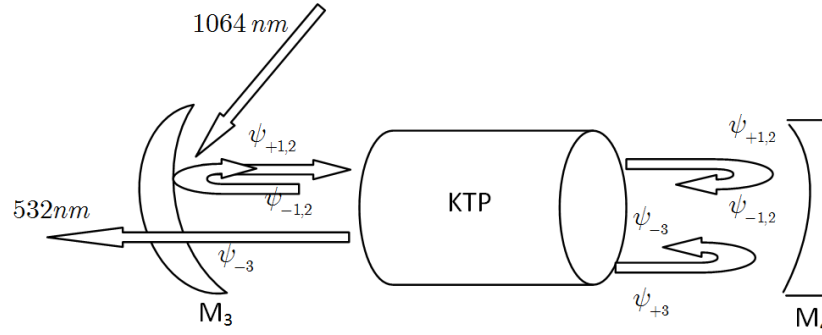

Fig. 1. A typical scheme of double-pass cavity for type II second harmonic generation.

4.2 Numerical procedure

The second harmonic generation equations, Eqs. (7)–(9), in essence, differ from the heat equation, Eq. (12). This is because the heat equation is a long transient diffusion equation and depends on time, while the wave equations do not. We should calculate the SHG output efficiency at any time until reaching the system to its steady-state. The numerical procedure adopted to solve eight equations simultaneously is as follows: at the first step, the wave equations are solved without coupling with heat and TIPM equations. Choosing appropriate Δr and Δz, i.e. space meshes, are of great importance in order to reach to accurate results in a logical time. Of course, the run time depends on computing facilities, but we are interested to adopt our calculations to common personal computers (in our case, an Intel CORE i5 processor). In the second step, the non-thermal results (fields without thermal effects) are put in the source of heat equation to calculate the temperature distribution of the crystal and then the TIPM as a function of time until temperature steady state. The latter (TIPM) is put in wave equations, in the exponential terms, to calculate the fields again but at various times. These fields are thermally affected. These thermally affected fields are return to the heat equation, and after calculating the temperature and TIMP, they again give to the wave equations. This procedure is repeated times ad times utile reaching to a stable solution for which the difference between same variables calculated in two successive iterations becomes smaller than a specific and very small value; say the tolerance which is chosen to be 1%. The iterations necessary for this calculations, depends strongly on the fundamental power and the beam spot size. Higher fundamental powers give rise to a higher temperature, so more iterations will conduct us to an accurate solution. On the other hand, smaller beam spot size needs finer Δr and consequently more CPU time. A part from parameters used, a subtle point lies in the wave equations and that is the transverse Laplacian. Our inspection, which was done for $\omega_f = 200 \mu m$, shows that ignoring the transverse Laplacian for small beam spot sizes does not bring in errors in physics of the problem, that is, the scattering of waves out of

the crystal is negligible. Notice that dropping out the transverse Laplacian results in no lateral boundary condition for the fields meaning no scattering. Surprisingly, this ignorance reduces the number of Δr significantly. For example, for $\omega_f = 200\,\mu m$, two set of (187, 1000, 222919) and (125, 200, 41373) for (r, z, t) meshes give the same results. However, the latter enormously reduces the computations time and necessary RAM. For $\omega_f = 50\,\mu m$, which is the case we emphasize on in this work, the situation becomes much more safer. In production of computational code, huge care has been made to avoid instability in, especially, heat equation and accuracy of solution. In particular, time step (Δt) is of much more importance. For $\omega_f = 50\,\mu m$ which is that used in Ref. [15], the best accurate results with the quickest run time were achieved when the crystal was divided into 500×200 ($r\times z$) meshes. The crystal temperature reaches to its steady state within an overestimated time of $1s$ for fundamental power up to 53 W. Appropriate time steps, which is dependent on Δr and Δz, have been found to be 231087, each with $1/231087\,s$. We wrote our code in Intel Fortran (ifort) and run it in LINUX operating system. Optimizations were performed to reduce the required RAM and CPU time, with the same results.

4.3 Numerical results

Figure 2 shows the forward, $|\psi_{+3}|^2$, and backward, $|\psi_{-3}|^2$, SHG efficiency along the crystal length for two fundamental beam spot sizes of $\omega_F = 50\,\mu m$ [15] (solid) and $\omega_F = 75\,\mu m$ (dashed). The total fundamental power which is divided equally between two orthogonal components, were taken to be $P_F = P^o + P^e = 53W$. As we will show later in this section, this power results in the maximum SHG efficiency at the presence of thermal effects. The figure, first, shows the benefit of double-pass cavity in which the fundamental and the second harmonic waves can continue their interaction towards a saturation situation. Second, the smaller beam spot size results in a higher efficiency. For $\omega_F = 50\,\mu m$, which is corresponding to Bai and Chen's experimental setup [15], a 40% SHG efficiency is obtained. The variations of the forward and backward fundamental waves, $|\psi_{\pm1}|^2$ or $|\psi_{\pm2}|^2$, versus z are plotted in Fig. 2 (right), showing how the fundamental waves exchange its energy into the second harmonic wave. Notice the fundamental as well as the second harmonic waves losses their energy also due to the absorption in the crystal. The longer crystal gives a better energy exchange and a higher SHG efficiency. This can be understood via the interaction length $l = \sqrt{\varepsilon_0 c^3 \pi \omega_F^2 n^{o,\omega} n^{e,\omega} n^{e,2\omega} / 4\omega^2 d_{eff}^2 P_F}$ which is 17 and $26\,mm$ for $\omega_F = 50$ and $\omega_F = 75\,\mu m$, respectively. With a $9\,mm$ length for KTP [15], the use of double-pass scheme doubles the effective length, allowing higher energy exchange.
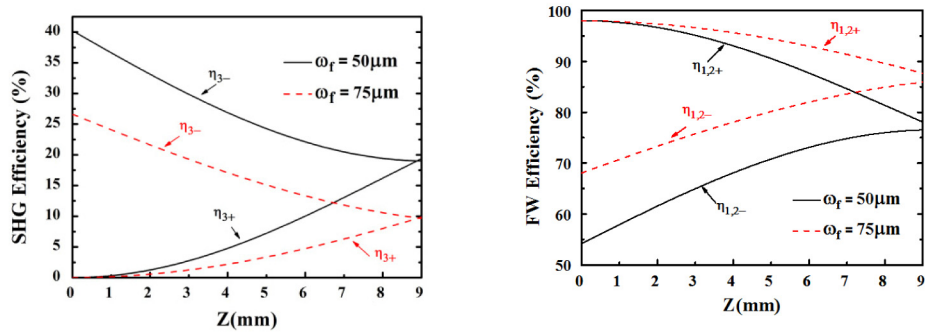
Fig. 2. The second harmonic generation efficiency (left) and the fundamental wave efficiency (right) along the crystal length affected by thermal effects.
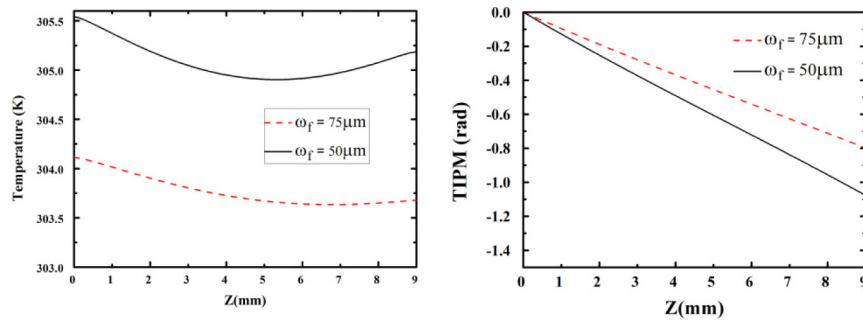

Fig. 3. (left) The temperature and (right) the thermally induced phase mismatching along the crystal length for P_F = 53 W and two beam spot sizes.
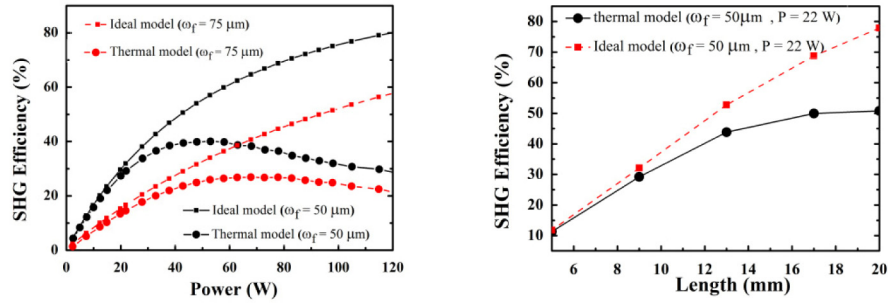

Fig. 4. (left) Two spot sizes of ω_F = 50 μm (solid) and 75 μm (dashed) have been compared with their ideal (non-thermal) cases. (right) the efficiency of SHG versus the crystal length for thermal case (solid) and for ideal case(dashed).

In order to provide a better insight into the problem, that is, why and how the SHG efficiency is reduced in the presence of thermal effects, we have plotted the temperature distribution and thermal induced phase mismatching in Fig. 3. Figure 3 (left) shows the temperature distribution along the crystal length at r = 0 for two beam spot sizes of $\omega_f = 50\,\mu m$ (solid) and $\omega_f = 75\,\mu m$ (dashed). Overall, the temperature is higher by $1.5\,K$ for smaller spot size. At $z = 0$, the temperature for both cases, shows somehow a higher value compared to other crystal points, which is attributed to the four times stronger

absorption coefficient of second harmonic waves. The end side, i.e. $z = l$, is also warmer than the middle parts, where the fundamental wave power is noticeably high (the residual fundamental power). This situation features a different trend compared to single-pass cavities in which the crystal is warmer in the middle parts of the crystal [23]. In fact, the reduction of SHG efficiency when crystal is warmed up, is blamed to the thermally induced phase mismatching illustrating in Fig. 3 (right). Although the temperature increase is moderate and is about $5.5\,K$, nevertheless a $-1.1\,rad$ mismatched phase is accumulated from the beginning to the end face of the crystal due to heat generated. This value is quite influential in SHG process.

In each experiment, efforts for achieving highest possible efficiency are made via adjusting the fundamental wave power and beam spot size. Figure 4 (left) shows the variations of SHG efficiency versus the input fundamental power for two beam spot sizes of $50\,\mu m$ (red-solid) and $75\,\mu m$ (black-dashed) for thermal model (big circles) and ideal model (small squares). In ideal model, the heat is uncoupled to the wave equations. The curves show higher SHG efficiency can be obtained if smaller beam spot sizes are used in both cases of thermal and ideal models. The deviations of thermal curves (circled-curves) from their ideal counterpart curves (squared-curves) occur by increasing the fundamental power. In the other word, thermal effect is manifested in powers strong enough to induce a sensible mismatched phase.

A comparison between our theoretical model and Bai and Chen's experimental work [15] shows a very good agreement. Bai and Chen by use of an active cooler where kept the crystal lateral side temperature to a constant value achieved an 25.5% efficiency for SHG at $22W$ of fundamental power. Our model yields an 29% efficiency at that fundamental power. A 3.5% difference is attributed to the cavity loss which has not been included in the model. Further investigation reveals that the efficiency can be further enhanced by increasing the fundamental wave input power, if crystal surface temperature can be kept constant. The solid curve for thermal case in Fig. 4 (left) indicates we can further obtain the SHG efficiency up to $\sim 39\%$ in the interval of 37 to $65W$ fundamental wave input power. Without thermal effects, the ideal model predicts 47% for $37W$ and 62% for $65W$ fundamental power. Our model predicted a noticeable reduction which is attributed to the TIPM. Notice in our model, we used perfect cooling [29], i.e. $T(t, r = a) = T_0$. Nevertheless, it could not prevent drops in SHG efficiency. This is because of a finite relaxation time (or finite thermal diffusivity) for heat transport from the central parts of the crystal to the cooled boundaries.

The crystal length effect on the SHG efficiency is worth examining when thermal effects present. Figure 4 (right), which is plotted for SHG efficiency as a function of crystal length, indicates that if we used a crystal with a length of $2\,cm$, with the specifications used by Bai and Chen in their experiment, a 40% SHG efficiency would be obtained, which is a saturated value.

The results presented so far describe the events after reaching the crystal temperature to its steady-state. It is worth completing the discussion with time evolution of temperature, TIPM, and SHG.
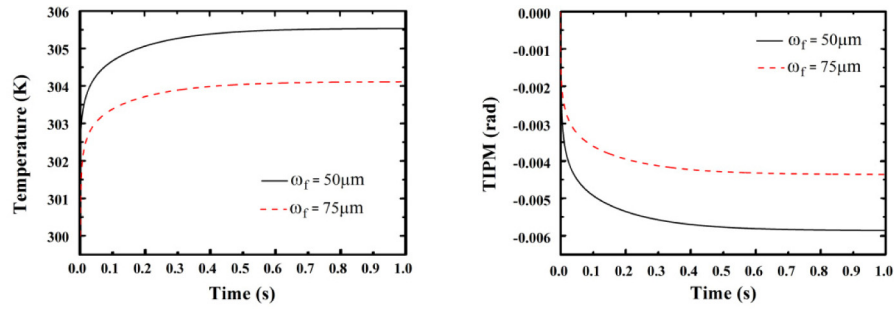
Fig. 5. (left) Time evolution of temperature change and (right) thermally induced phase mismatching for two beam spot sizes.

Figure 5 (left) shows the time evolution of temperature and (right) the thermally induced phase mismatching when going towards their steady-state at the end face of the crystal. Approximately, after 1 second that is a specific value for KTP, the system reaches to its steady-state. Increase in the temperature which is accompanied by an induced phase mismatching, leads to a drop in SHG efficiency in time. Figure 6 shows how the SHG efficiency decreases in time when going towards its steady-state. Reduction in SHG efficiency from 50% to 40% for $\omega_F = 50\mu m$ and from 31% to 26% for $\omega_F = 75\mu m$, both for a $53W$ fundamental power, happens due to thermal effects.
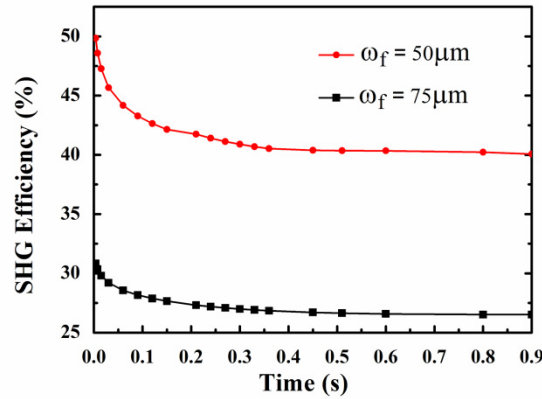

Fig. 6. The time evolution of SHG efficiency for two beam spot sizes of $\omega_F = 50$ μm (red curve) and $\omega_F = 75$ μm (black curve) for 53 W fundamental power.

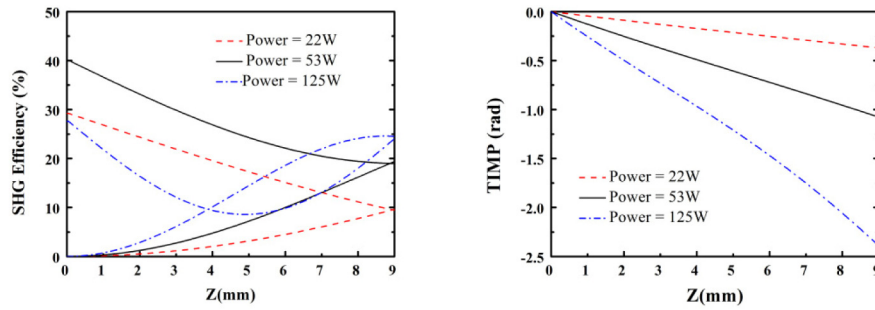Fig. 7. (left) Second harmonic generation efficiency and (right) thermally induced hase mismatching for three fundamental input powers.

The last part is devoted to examine two other powers, one less than and other higher than the optimum power, say $53W$, to see how they result in lower SHG efficiencies. Figure 7 (left) shows the variations of SHG efficiency, $\eta_{3\pm}$, for $125W$ (dashed-dotted), $53W$ (solid), and $22W$ (dotted) fundamental powers. For $22W$, forward and backward SHG do not saturated at $z = l$ and $z = 0$, respectively, because this power lead to an interaction length longer than twice the crystal length. Therefore, longer crystal is needed in this case, since the interaction is raw. On the other hand, for $125W$ pump power for which the interaction length shortens, strong TIPM drops in SHG efficiency. Figure 7 (right) illustrates the corresponding TIPM; for $125W$, TIPM is about $-2.4\,rad$ which is strongly destructive. These results emphasize an optimization between crystal length, fundamental input power, and beam spot size to get the highest possible efficiency in second harmonic generation.

5. Conclusion

In conclusion, we presented an eight-coupled model to include thermally induced phase mismatching and thermal lensing in double-pass continuous-wave type II second harmonic generation with Gaussian waves. Our model could explain the reduction in SHG efficiency when heat is generated in the nonlinear crystal. Our model could successfully regenerate the experimental data reported already by Bail and Chen for a double-pass continues-wave SHG setup [15]. In spite of the presence of thermal effects, the model predicts higher SHG efficiencies for smaller beam spot sizes can give. However, the highest possible efficiency can be obtained by optimizing beam sot size, fundamental input power, and crystal length. For a crystal with specific length, the fundamental power and the beam spot size must be precisely adjusted to get the highest SHG efficiency. The subtle point in such systems is a competition between the interaction length and thermally induced phase mismatching. Although higher intensities decrease the interaction length, but it could increase TIPM increases leading to drop in efficiency.

Acknowledgment